AIChE WILEY InterScience DISCOVER SOMETHING GREAT

PARTICLE TECHNOLOGY AND FLUIDIZATION

Solid Flow Rate Prediction in Silo Discharge of Aerated Cohesive Powders

Diego Barletta, Giorgio Donsì, Giovanna Ferrari, Massimo Poletto, and Paola Russo
Dipartimento di Ingegneria Chimica e Alimentare, Università degli Studi di Salerno
Via Ponte Don Melillo, I-84084 Fisciano (SA), Italy

DOI 10.1002/aic.11212
Published online July 17, 2007 in Wiley InterScience (www.interscience.wiley.com).

Aerated discharge of six cohesive powders differing in particle size, density and flow properties is presented. These samples were characterized by means of fluidization experiments and rheology shear tests carried out in a ring shear tester. In the silo discharge experiments the measurements of the discharge rates and the mass of residual solids as a function of the aeration rate were carried out. In addition, photographic techniques highlighted the aggregative behavior of these powders. Solids aggregates, in fact, were visible within the aerated beds of solids during the fluidization experiments and in the streams of the discharging solids. Experimental data on powder flow properties and on fluidization were analyzed in order to evaluate aggregate diameters. These values compared fairly well with the aggregate diameters observed and allowed evaluation of the voidage values external to the aggregates. These results were used in a modified form of the De Jong and Hoelen equation to predict the solid discharge rate with reasonable accuracy. A modified version of this procedure has been proposed to evaluate the aggregate density and diameter starting from the vibrated density of the powder. This makes preliminary powder fluidization experiments unnecessary in the estimation of the solid discharge rates. © 2007 American Institute of Chemical Engineers *AIChE J,* 53: 2240–2253, 2007

Keywords: Solid flow rate, aerated powders, silo discharge, cohesive powders, fluidization, powder flow properties

Introduction

The discharge of fine powders from hoppers is hindered by either fluid dynamic interactions (see Crewdson et al.[1]) or cohesive interparticle interactions. The discharge rate of these powders, in fact, is overestimated by the Beverloo et al.[2] equation

$$W_s = 0.58(1-\varepsilon_b)\rho_p\sqrt{g(d_o - 1.5d_p)^5} \qquad (1)$$

where W_s is the solids discharge rate, ε_b is the voidage of the bulk solids, ρ_p and d_p are the density and the mean diameter of the solid particles, d_o is the outlet diameter and g the acceleration due to gravity. The significance of fluid dynamic and cohesive interactions depends mainly on the particle diameter. Fluid dynamic interactions appear to be significant for particle diameters, which are somewhat larger than those for which cohesive interparticle forces appear to be effective. The Geldart[3] classification valid for fluidization was extended by Geldart and Williams[4] to include the discharge behavior of powders. Accordingly, Group A powders can be referred to as those for which fluid dynamic interactions affect the discharge, Group C powders as those for which cohesive forces can produce irregular flow. Our attention will be focused on cohesive powders here on.

Correspondence concerning this article should be addressed to M. Poletto at MPOLETTO@UNISA.IT.

The effects of cohesive forces on powder discharge also depend on powder consolidation. Such effects primarily consist of arching and rat-holing phenomena. An evaluation of the storage conditions that can produce such phenomena was first given by Jenike.[5]

The injection of air can produce favorable effects in the flow of fine powders producing gas pressure gradients favorable to the solids flow. In particular, for Group C powders, aeration may break arches and pipes and determine the flow of powders blocked at zero air flow rate. Air can be injected in different ways such as near the outlet of conical hoppers[6] or through the flat bottom of bins.[7] Various attempts have been made to obtain valid equations for the correlation of the discharge rates of free flowing solids at the different operating conditions corresponding to low,[1] intermediate,[8,9] and elevated[10] aeration rates. Some terms appearing in these equations, such as the pressure gradient in proximity of the hopper outlet or the air flux through the same orifice, appear difficult to evaluate. Moreover, from experiments carried out in similar aerated discharging devices on free-flowing[11] and cohesive powders,[12] it appears that a different discharge behavior is found in the two cases.

Experiments on a corn starch powder[13] demonstrated that the first effect of aeration is the breaking up of arches at the outlet, and the prevention of their subsequent formation. At low and slightly increasing aeration levels this powder shows rat-holing and core flow (funnel flow), respectively. The effect of solids flow promotion by increasing aeration is to mobilize the superficial layers of solids involved in the funnel flow mechanism. Only very high-aeration rates are able to fluidize the solids and to produce flow fields similar to those found with aeratable powders at high-aeration. Despite such complex phenomenology, the discharge rate for that powder under aeration is not very different from that predicted by the models mentioned previously. According to Donsì et al.,[13] it is possible to apply some simplifications that allow the use of the De Jong and Hoelen[9] equation in a predictive way. Indeed, according to De Jong and Hoelen[9] the solid-discharge rate can be expressed as follows

$$W_s = 0.55\rho_p(1-\varepsilon_b) \times \left[a\left(\frac{Q_{fo}}{\varepsilon_b} - \frac{Q_{so}}{1-\varepsilon_b}\right)^2 + b\left(\frac{Q_{fo}}{\varepsilon_b} - \frac{Q_{so}}{1-\varepsilon_b}\right)\right]^{0.5} \quad (2)$$

where

$$a = \frac{1.75}{12}\frac{\rho_f d_o}{\rho_p d_p \varepsilon_b}\left(1 - 1.5\frac{d_p}{d_o}\right)^4,$$

$$b = \frac{150}{8}\frac{\pi\mu_f d_o^3(1-\varepsilon_b)}{\rho_p(d_p\varepsilon_b)^2}\left(1 - 1.5\frac{d_p}{d_o}\right)^4,$$

Q_{fo} and Q_{so} are the volumetric flow rates of the gas and of the solid through the outlet orifice, ρ_f and μ_f are the gas density and viscosity. Some estimates based on gas pressure profiles allowed us to verify that during the discharge, the amount of air percolating through the bed is negligible in the gas-mass balance, and, therefore, the gas rate through the orifice is equal to the sum of the aeration rate Q_f, and of the interstitial air brought by the solids, that is

$$Q_{fo} = Q_f + Q_{so}\varepsilon_b/(1-\varepsilon_b) \quad (3)$$

Furthermore, it can be observed that no effect of gravity is included in Eq. 2, and, therefore, by comparison with Eq. 1 and use of Eq. 3, it can be modified into

$$W_s = 0.55\rho_p(1-\varepsilon_b) \times \left[a(Q_f/\varepsilon_b)^2 + bQ_f/\varepsilon_b + g(d_o - 1.5d_p)^5\right]^{0.5} \quad (4)$$

The comparison between Eq. 4, and the experimental results obtained with both slightly cohesive powders and aeratable powders is satisfactory. However, the aforementioned discussed framework changes if we use powders with poor flow properties. In particular, Donsì et al.[14] worked with cohesive magnesium carbonate powders for which Eq. 4 largely overestimates solids discharge rates. Nevertheless, it was possible to obtain a better agreement by assuming that these powders do not flow as single particles but as aggregates. These, in fact, play a key role in the determination of effective powder permeability. The theoretical framework in which all these phenomena can be qualitatively and quantitatively accounted for will be discussed in the following section.

Powder aggregation is a well known phenomenon in fluidization. According to Wang et al.[15] the most common type of fluidization curve of cohesive powders shows the well known linear section of pressure drop, increasing at increasing aeration velocity. When the pressure drop overcomes the bed weight and its adhesion forces to the container walls, the bed material starts moving like a plug. When the plug is broken, a marked pressure drop reduction is observed corresponding to the formation of large aggregates. These are characterized by significant void spaces between them that allow low-pressure drops over wide velocity ranges. These appear as wide local minima in the fluidization curve. At large aeration rates, in fact, aeration is generally sufficient to resuspend and possibly breakup the aggregates to determine proper powder fluidization, as observed by Wang et al.[15] and Pacek and Nienow.[16] Pressure drops lower than the bed weight could also be found at decreasing aeration rates and were attributed to some partial adhesion of particle aggregates to the column walls.[17] The hypothesis of agglomerate fluidization is frequent in literature, and has also been introduced to explain the effects of the techniques inducing homogeneous fluidization of cohesive powders (see for example Russo et al.[18]). Fluidization curves of starches in Figures 7 and 8 described in the Results Section follow the phenomenology reported before. According to Wang et al.,[15] other cohesive powders, such as limestone, on the other hand, may fluidize properly at low-aeration rates, and give rise to significant channeling phenomena at the higher aeration rates, which determine progressive powder defluidization. The powders studied in the aerated discharge by Donsì et al.[14] and the silica and carbonate powders discussed in the Results section (Figures 5, 6 and 7) belong to this category. Despite channeling during fluidization, however, their discharge from silos assisted by aeration could be properly described assuming aggregative behavior.

The purpose of this work is to validate the procedure proposed by Donsì et al.[14] to estimate powder discharge for a number of different cohesive powders. According to this procedure powder flow properties are measured with a shear tester and powder permeability is evaluated from fluidization experiments in order to estimate aggregate densities and diameters. In this respect, the possibility of evaluating discharge rates of aerated solids, without necessarily carrying out fluidization experiments, will also be verified in this article.

Theoretical Background

In their analysis of aerated discharge, Donsì et al.[14] assumed a similar mechanism for aggregate formation both in fluidization and aerated discharge of cohesive powders. The hypothesis is that aggregates detach themselves along almost horizontal surfaces. In the case of fluidization this process can start from horizontal cracks forming when the beds starts to expand. In these conditions aggregates can form by detaching from the bulk in the lower portion of the slugs wherever the aggregate weight overwhelms the attraction force, F_c, of the contact between the aggregate and upper lumps of the solids. Aggregate formation, therefore, should proceed by separation of aggregates one by one from the bed bottom toward the top. Similarly, in aerated discharge a region develops close to the outlet where the powder expands in its downward motion toward the outlet itself. Here a stationary and almost vertical powder expansion profile develops where the aggregates may form due to the occurring loss of support from the layers below. For both fluidization and discharge, with the assumption of spherical aggregates, the force balance on the detaching aggregate is

$$\frac{\pi d_a^3}{6}\rho_p(1-\varepsilon_i)g = F_c \tag{5}$$

where d_a and ε_i are the aggregate diameter and its internal voidage. In principle, Eq. 5 should also include some other force contributions accounting for fluid dynamic forces. However, it is likely that, due to local voidage inhomogeneities, these forces might be significantly lower than the particle weight according to the local gas velocity. In any case, being close to the fluidization condition these forces are of the order of magnitude of the gravity force, and, therefore, Eq. 5 provides a correct estimation of the range of forces involved in the aggregate formation. The value of F_c should be related to the bulk properties of the powder and, in particular, to its tensile strength. When the aggregates are compacted, in fact, the relationship between the tensile stress σ_t and F_c, might be described by the force balance across a plane separating two aggregate layers

$$\sigma_t = F_c n_c \tag{6}$$

where n_c is the contact density between aggregates in neighboring layers that, in turn, can be expressed as

$$n_c = k d_a^{-2} \tag{7}$$

where k is the number of effective contacts between an aggregate and its neighbors on another layer. Empirical functions $k(\varepsilon)$ were developed by authors, such as Rumpf[19] and Kendall et al.[20] in the case of packing of rigid spherical particles. In this case, the maximum value for k at the minimum allowed voidage provided by both the authors was about three. This value is close to the maximum reasonable value for almost round objects belonging to two neighboring layers and touching each other. Therefore, it can be assumed to apply also in the case of the aggregates. Combining Eqs. 5 to 7, it is possible to correlate the aggregate size starting from the bulk tensile strength of the powder

$$\frac{\pi d_a^3}{6}\rho_p(1-\varepsilon_i)g = \frac{\sigma_t d_a^2}{k} \tag{8}$$

If we assume for the powder an ideal Coulomb elastic-plastic solid behavior, its yield condition on a generic plane is given in terms of normal stress, σ, and shear stress, τ. Namely, the yield will follow the equation

$$\tau = \sigma \tan\phi + c \tag{9}$$

where ϕ is the angle of internal friction, and c is the cohesion. Accordingly, the tensile strength σ_t will be given by the following equation

$$\sigma_t = -\frac{2c\cos\phi}{1+\sin\phi} \tag{10}$$

Equation 10 is given by the intersection with the σ-axis of the Mohr circle representative of the stress state in the yielding powder subject to pure uniaxial tensile stress, which is the circle tangent to the yield locus on the tensile side and passing through the origin. Both the cohesion c and the angle of internal friction ϕ are functions of the powder consolidation. Assuming that consolidation is very low inside an aerated powder, Donsì et al.[14] used for c and ϕ in Eq. 10 the extrapolation to zero consolidation of these parameters measured with a shear cell. Figure 1 reports an example of this procedure for the calcium carbonate powder described in the Materials section.

Equation 8 can be solved for the aggregate diameter if the aggregate internal voidage or the aggregate density is known. Donsì et al.[14] proposed a procedure based on fluidization data, assuming that powder expansion and aggregation state at the silo opening are set by aeration before opening. According to this procedure the distribution of the solids mass in the aggregates m_s, is

$$m_s = \rho_p(1-\varepsilon_i)(1-\varepsilon_e)\Sigma H \tag{11}$$

where ε_i is the voidage within the aggregates, and ε_e the voidage between the aggregates Σ, and H the bed cross-section and the bed height. The mass balance on the gas is

$$u = u_e\varepsilon_e + u_i\varepsilon_i(1-\varepsilon_e) \tag{12}$$

where u is the gas superficial velocity, u_e is the gas velocity in the voidage external to the aggregates, and u_i the

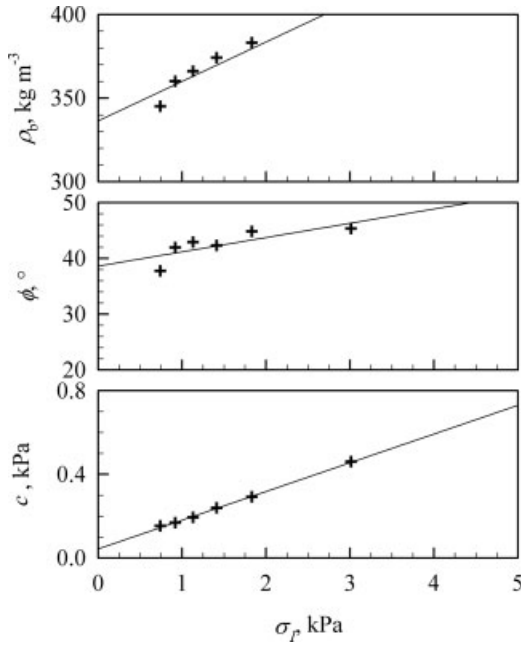

Figure 1. Example of estimation of powder properties at zero consolidation for bulk density, static angle of internal friction and cohesion carried out for the calcium carbonate powder.

gas velocity within the aggregates. The pressure drops through the aggregates and around them should be equal to the measured value of ΔP. Therefore, within the aggregates and according to the Ergun equation for viscous regimes, we have

$$\frac{\Delta P}{H} = 150\frac{\mu_f u_i}{d_p^2}\frac{(1-\varepsilon_i)^2}{\varepsilon_i^3} \tag{13}$$

while outside the aggregates, according to the Ergun equation for intermediate regimes, it is

$$\frac{\Delta P}{H} = 150\frac{\mu_f u_e}{d_a^2}\frac{(1-\varepsilon_e)^2}{\varepsilon_e^3} + 1.75\frac{\rho_f u_e^2}{d_a}\frac{1-\varepsilon_e}{\varepsilon_e^3} \tag{14}$$

In principle, the set of five Eqs. 8 and 11 to 14 can be solved for each fluidization condition independently in order to evaluate the five unknown variables d_a, ε_i, ε_e, u_i and u_e. However, recognizing that the internal voidage of aggregates and the aggregate diameter are powder properties that should not depend on aeration, a different procedure was proposed by Donsì et al.[14] According to this procedure, a unique value of ε_i could be found by using a regression procedure on all fluidization/expansion data in which the bed appears completely fluidized. In this procedure the objective was to find the best choice for ε_i, which minimizes the sum of relative square deviations between diameters evaluated for each powder according to Eq. 8, and those evaluated for the same powder solving the system of Eqs. 11 to 14 at each aeration rate in the fluidization range. The aggregate density can be evaluated from the internal voidage

$$\rho_a = \rho_p(1-\varepsilon_i) \tag{15}$$

Another possible approach can be adopted to evaluate the aggregate diameter and the bed external voidage if an estimate of the aggregate density, ρ_a is known. In this case from Eq. 8 it is

$$d_a = \frac{6}{k\pi}\frac{\sigma_t}{g\rho_a} \tag{16}$$

and the external voidage can be evaluated from the powder bulk density

$$\varepsilon_e = \left(1 - \frac{\rho_b}{\rho_a}\right) \tag{17}$$

According to Donsì et al.[14] at the outlet the powder discharges in the form of aggregates rather than as single particles. Therefore, a modified form of Eq. 4 in which the particle diameter d_p, the particle density ρ_p, and the bed voidage ε_b, are substituted by the aggregate diameter d_a, the aggregate density ρ_a, and the voidage external to the aggregate ε_e, respectively (ε_e being the voidage effectively available for gas flow)

$$W_s = 0.55\rho_a(1-\varepsilon_e)\left[a'(Q_f/\varepsilon_e)^2 + b'Q_f/\varepsilon_e + g{d_o}^5\right]^{0.5} \tag{18}$$

and

$$a' = \frac{1.75}{12}\frac{\rho_f d_o}{\rho_a d_a \varepsilon_e}, \quad b' = \frac{150}{8}\frac{\pi\mu_f d_o^3(1-\varepsilon_e)}{\rho_a(d_a\varepsilon_e)^2}$$

In Eq. 18, the terms accounting for the outlet contraction due to the finite size of particles, that are visible in Eq. 2, are neglected. It should be considered, in fact, that aggregates can breakup, and that the orifice edges do not interfere significantly with their motion and the resulting mass-flow rate.

Experimental Setup

Apparatus

The aerated bin used is shown in Figure 2. The bin had cylindrical walls 3 mm thick, made of transparent perspex to allow visual inspection of the inside. It was 520 mm high, and 147 mm ID. At the bottom of the bin there was a gas distributor (D), consisting of a 10 mm thick sintered plate made of a 10 μm brass powder. The wind box (WB) below the distributor was made of stainless steel, and was provided, in the middle, with a vertical duct for the discharge of solids shaped as an inverted funnel. An interchangeable orifice (◯), was mounted at the top of this duct, at the distributor level. This device allowed some space between the discharging solids and the duct wall, and, therefore, allowed atmospheric pressure around the falling solids in order to avoid "stand pipe effects". At the exit of the duct a sliding valve (S), which was operated pneumatically, was used to close the outlet, while loading the solids

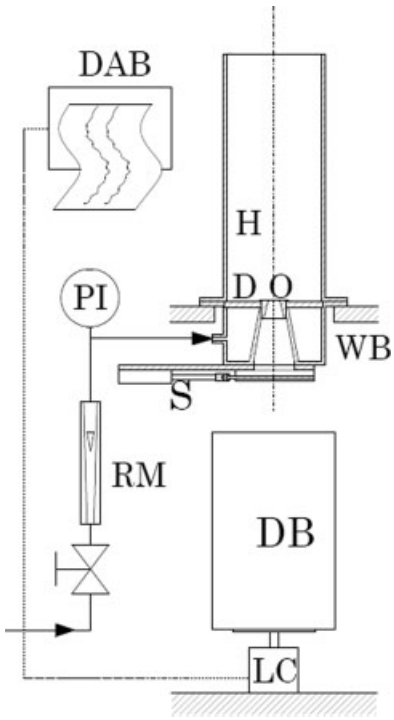

Figure 2. Experimental apparatus: D, gas distributor; DAB, data acquisition board or chart recorder; DB, discharge bin; H, bin; LC, load cell; O, outlet orifice; PI, pressure indicator; RM, rotameter; S, slide lock; T, tube; WB, wind-box.

inside the bin. The discharged solids were collected in a bin (DB), placed on a load cell (LC), based on a strain gage bridge, operating in the range 0–50 N. The air flow rate through the distributor was regulated by a valve, and measured with a rotameter (RM). Before entering the system, the air was dehumidified in a refrigerated unit.

The fluidization curve of the powders was measured in a 52 mm ID glass column fitted with a pressure tap located on the wall just above the sintered-glass distributor. A graduated scale fit on the column side was used to measure the bed height by direct inspection. Corn starch powders tended to form stable plugs in the small glass column, and, therefore, were fluidized directly in the aerated silo bin with the outlet closed.

The powders flow functions were measured by a Schulze[21] ring shear tester. This tester is provided with a kinematic chain designed and built to support the weight of the cell lid, and, therefore, it was possible to carry out shear stress measurement at low-consolidation levels.

Materials

Six different cohesive powders were used in the experiments. Powder densities and main diameters of particle-size distributions are reported in Table 1. Scanning electron microscopy pictures of these powders at different magnification ratios are shown in Figure 3.

The particle-size distribution of the 15 μm magnesium carbonate powder and of silica was bimodal. The first showed two peaks at 3 and 20 μm, the second two peaks at 4 and 50 μm. The particle-size distribution of the other powders was unimodal. The bulk density of a bimodal particle-size distribution can vary significantly if the finer particles tend to fill the voidages left by the larger ones (see for example[22,23]). The particle-size distribution and the fluidization behavior assign all these powders to group C of the Geldart[3] classification. The flow functions of these powders, which are reported in Figure 4, also indicate that their flow behavior is generally in the range of cohesive and very cohesive powders. In particular silica and carbonates fall in the very cohesive range, while starches fall in the cohesive range. The values of bulk density, angle of internal friction and cohesion corresponding to zero consolidation are reported in Table 1. All these values were measured with the standard Schulze cell, and extrapolated to zero values of the major principal stress during consolidation σ_1. Vibrated bulk densities of the materials were obtained by filling a graduated plastic container of about 50 mL with a known amount of powder, and vibrating it until constant volume, and, therefore, constant bulk density were attained.

Procedures

Fluidization. The column was loaded from the top through a funnel or with a spoon in a relatively loose state. Increasing steps of the aeration rates were carried out in order to evaluate stationary bed heights and pressure drops. In order to obtain relevant results, the process was carried out in an aeration velocity range comparable to the one used in the discharge experiments. When the highest aeration rate was attained, the procedure continued by decreasing in stepwise mode the aeration rate until zero flow was obtained.

Table 1. Material Properties

Material	ρ_p kg m^{-3}	a_s m^{2}g^{-1}	d_p μm	d_{pv} μm	d_{p10} μm	d_{p50} μm	d_{p90} μm	ρ_{bv} kg m^{-3}	ρ_{b0} kg m^{-3}	c_0 Pa	ϕ_0 deg	σ_t Pa	*Sym.*
Calcium Carbonate	2539	1.5	4.1	15	1.9	6.7	40	421	336	43.0	38.6	41.4	+
Magnesium Carbonate 4 μm	2600	2.2	2.7	5.3	1.3	4.1	10	833	679	61.4	41.3	55.6	▽
Magnesium Carbonate 15 μm	2600	1.7	3.5	17	1.2	15	39	1290	886	20.7	36.7	20.8	△
Silica	2650	0.75	7.6	28	2.8	21	66	1400	1020	43.3	36.7	43.4	○
Potato Starch	1572	0.28	21	48	23	46	80	854	773	24.2	25.3	30.7	□
Corn Starch	1200	0.34	18	19	15	46	102	568	505	46.8	35.2	48.5	◇

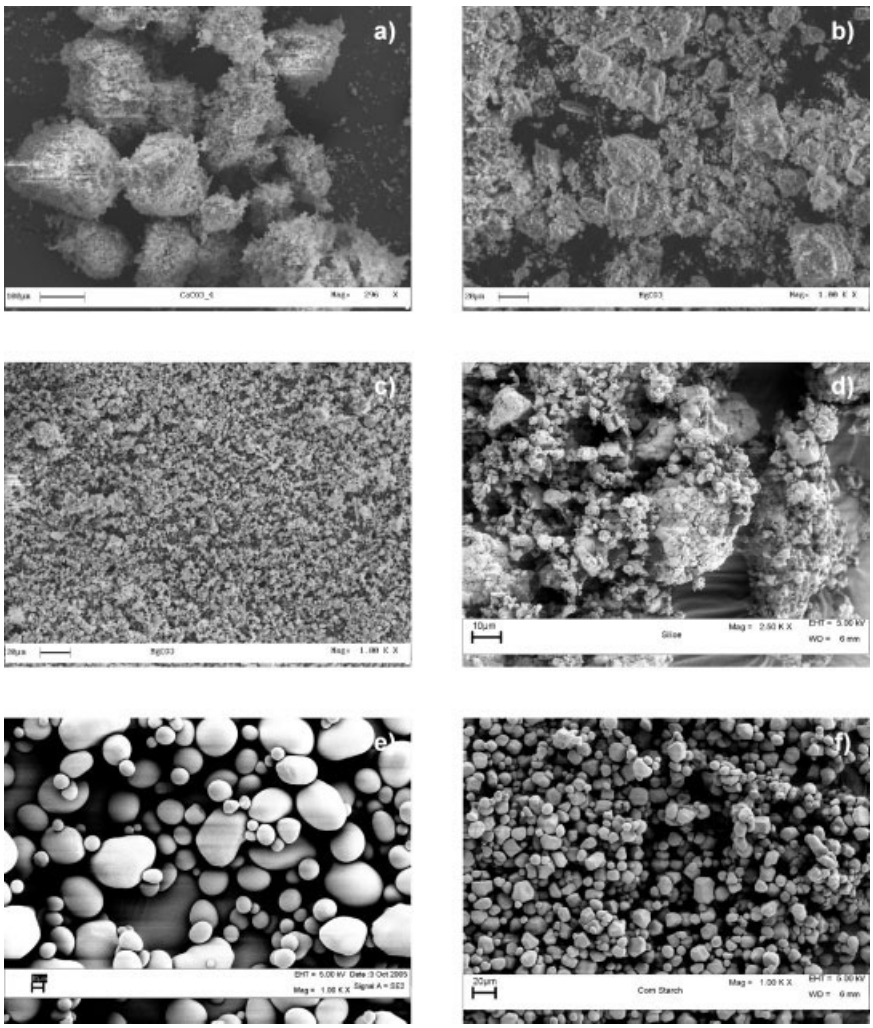

Figure 3. SEM images of the powders tested: (a) calcium carbonate; (b) magnesium carbonate 15 μm powder; (c) magnesium carbonate 4 μm powder; (d) silica; (e) potato starch and (f) corn starch.

Bed masses and corresponding static bed heights used in the fluidization experiments are reported in Table 2.

Aerated Discharge. The bin was loaded from the top through a funnel connected to a large perspex tube, which was plunged into the bin for the two magnesium carbonates and the corn starch powders. Calcium carbonate, silica and potato starch powders, on the other hand, were loaded with the help of a spoon. Bed masses and corresponding static bed heights used in the aerated discharge experiments are reported in Table 3. After the silo loading, the aeration rate was set. After a period of time long enough to be sufficient for the bed to reach stationary aeration conditions, the silo slide at the outlet was opened. Time series of the mass of discharged solids measured by the load cell, LC in Figure 2, were acquired by a PC with a data acquisition board (DAB). Further experiments were carried out to obtain images of the discharging streams of solids below the outlet. In these experiments a digital camera and a stroboscopic light were used to "freeze" the motion of the discharging solids. In order to have a single light pulse during the exposure, the period between subsequent flashes of the stroboscopic light was regulated to be the same as the exposure time.

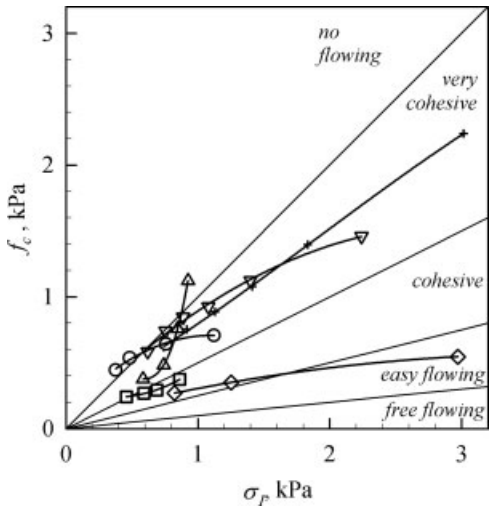

Figure 4. Flow functions of the powder tested with the powder classification as given by Jenike.[5]

Symbols are summarized in Table 1.

Table 2. Test condition for Fluidization Experiments

Material	D_c mm	m_b kg	H mm
Calcium Carbonate	52	0.110	150
Magnesium Carbonate 4 μm	52	0.210	140
Magnesium Carbonate 15 μm	52	0.300	135
Silica	52	0.334	140
Potato Starch	52	0.267	140
Corn Starch	147	3.50	430

Results

Fluidization curves

The fluidization curves of the materials tested were determined following the procedure suggested by Donsì et al.[14] to estimate the aerated discharge of solids. This procedure has described in the Theoretical Background section. All the materials tested show some hysteresis providing different bed expansion and gas-pressure drop in experiments with increasing or decreasing velocity. This behavior was already known and carefully described by Wang et al.[15] There is not a general rule on whether the bed expansion or pressure drop curve line in the decreasing aeration rate branch are lower or higher than the increasing branch. What is generally observed is that the decreasing branch of the fluidization curve is smoother than the increasing branch. In the authors' experience, the results of decreasing velocity experiments are also more reproducible than those of increasing velocity experiments. However, it ought to be noted that the purpose of the fluidization experiment is to evaluate the permeability of the aerated bed during discharge, and the procedure followed for the discharge experiments is more similar to the increasing aeration experiment. It was verified, in fact, that fluidization and bed expansion data obtained with increasing aeration rates provide model results that are better than those obtained with decreasing aeration. For all these reasons, in this section we will show only the increasing branches of the fluidization and bed expansion curves from Figures 5 to Figure 8. Figures 5 and 6 show the fluidization curves and the bed expansion curves for the carbonates. These curves show several similarities shared also with those of silica reported in Figure 7. At low-aeration rates, pressure drops increase up to gas-superficial velocities, at which a maximum of pressure is observed between 1.2 and 1.4 times the bed-weight value. Pressure drops larger than the bed weight corresponded to the formation of a rising plug, like the one shown in Figure 9a for the silica powder. The plug could be kept within the column only by breaking it. Generally the plug was not one single piece, but had several horizontal cracks across its every few centimeters. Figure 9b shows this behavior for the finer magnesium carbonate powder. After the slug formation and breakage, a velocity range is found in which the pressure drop equals the bed weight, and, therefore, the powder could be considered fluidized despite the absence of evident powder motion. Closer inspection of the bed revealed an evident network of cracks defining aggregates of a few millimeters in diameter. Figure 9c shows an example of this behavior for coarser magnesium carbonate powder. The finer magnesium carbonate powder, before expanding and being considered fluidized, showed a fairly wide velocity range of unstable slugs. In this regime pressure drops fluctuated between values equal to the bed weight and 10% higher. For all the powders, at the highest gas velocities the pressure drops decreased at values that are about 30–40% lower than the bed weight, suggesting the onset of channeling phenomena and partial defluidization. However, the bed of carbonates also continued to expand in this aeration range. A typical channeling region at high-aeration is shown in Figure 9d, for the coarser magnesium carbonate powder, where the high-gas shear action smoothes the aggregate shapes. Fluidization curves of starches shown in Figures 7 and 8 show the typical behavior, with a marked minimum at intermediate aeration velocities, that was widely described in the introduction and can be attributed to the defluidization of the aggregates formed after the bed suspension at lower aeration rates.

Discharge experiments

Time series of the discharged mass of solids were obtained at different aeration rates. An example of these is reported in Figure 10, which was obtained for the coarser magnesium carbonate powder at a nominal aeration velocity $u = 21$ mm s^{-1}. Some common features of mass-time series can be summarized. During the initial stages of the discharge, it was possible to identify a peak in the load trace due to the impact in the collecting bin of the solids contained in the diverging channel above the slide lock. Next, an almost stationary discharge rate (appearing as a linear section of the curve in Figure 10) was observed in the first part of the discharge experiment. It was only in the last part of it, that it was possible to

Table 3. Test Condition for Aerated Discharge Experiments

								Model symbol		
Material	D_s mm	m_s kg	H mm	d_o mm	d_a mm	$s(d_a)$ %	ρ_a kg m^{-3}	*Single particle*	*Aggregate/ fluidization*	*Aggregate/ Vib. Dens.*
Calcium Carbonate	147	2.2	370	30	6.4	16	419			
Magnesium Carbonate 4 μm	147	3.9	370	13	4.4	39	939			
Magnesium Carbonate 15 μm	147	5.2	370	13	1.1	21	1180			
Silica	147	5.9	370	13	2.7	62	1037			
	147	6.6	370	30	2.7	62	1037			
Potato Starch	147	4.1	370	13	2.2	15	936			
Corn Starch	147	3.0	430	13	6.1	10	516			

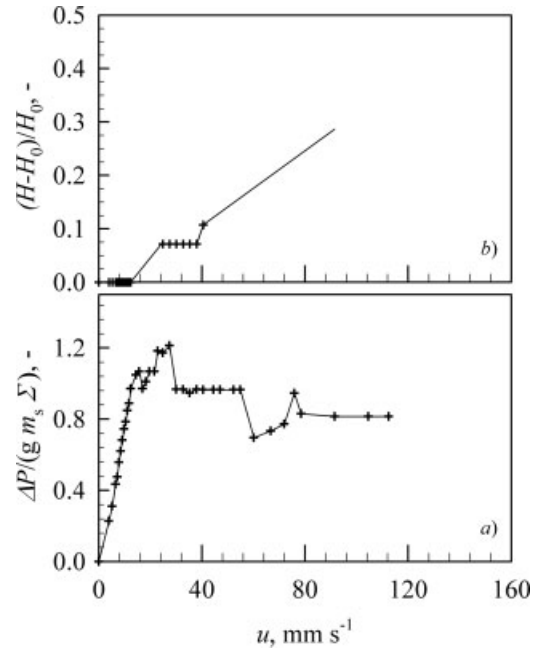

Figure 5. Fluidization and expansion curve for calcium carbonate powder in a 52 mm ID fluidization column.

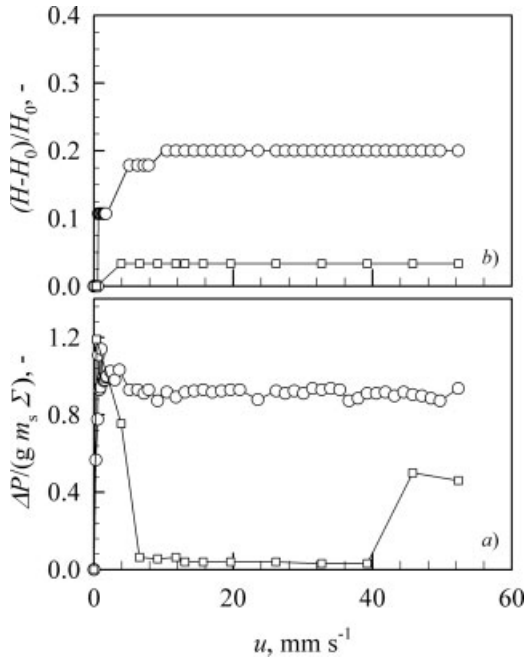

Figure 7. Fluidization and expansion curve for silica and potato starch powders in a 52 mm ID fluidization column: ○, silica; □, potato starch.

observe a reduction of the solids discharge rate, appearing as a convex portion of the discharge curve in Figure 10. The data in the time intervals during which stationary discharge rates were observed were used to evaluate solids discharge rates. As an example in Figure 10, the data range adopted is that contained in the hatched area and the dashed line derives from the linear interpolation of data in this range. At all aeration conditions, solids discharge rates were assumed to be the slopes of the interpolating lines in the constant discharge rate region.

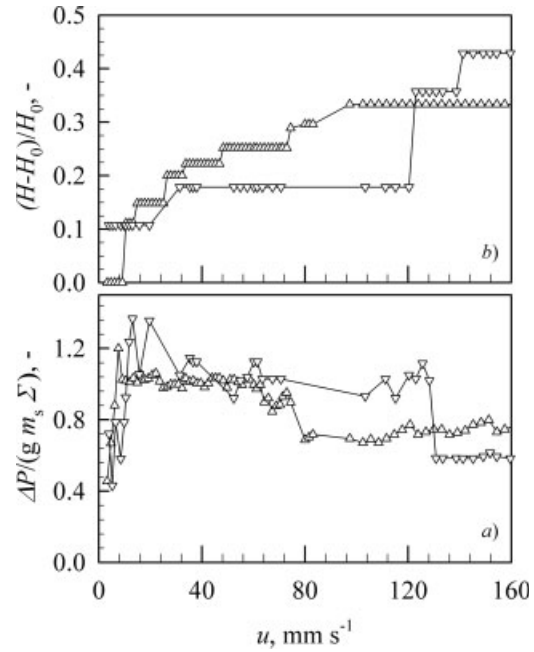

Figure 6. Fluidization and expansion curve for magnesium carbonate powders in a 52 mm ID fluidization column: △, 15 μm powder; ▽, 4 μm powder.

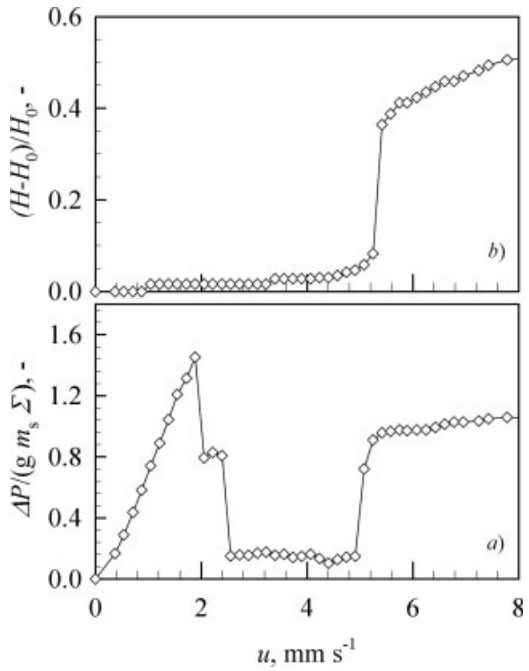

Figure 8. Fluidization and expansion curve for corn starch powder in a 147 mm ID fluidization column.

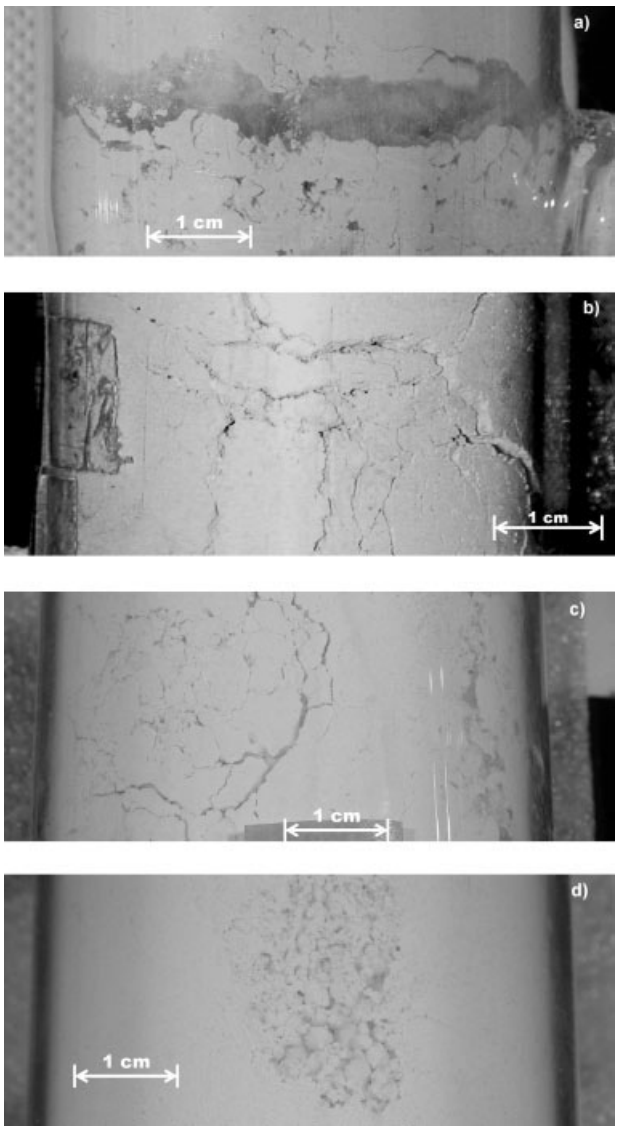

Figure 9. Aggregation during aeration for some of the tested powders: (a) silica, u = 1.0 mm s^{-1}; (b) 4 μm magnesium carbonate, u = 114 mm s^{-1}; c) 15 μm magnesium carbonate, u = 27.9 mm s^{-1}; (d) 15 μm magnesium carbonate, u = 120 mm s^{-1}.

Table 3 summarizes the main test parameters of the solids discharge experiments. Experimental results in terms of solids discharge rates are reported as a function of aeration in Figure 11a for carbonates, in Figure 12a for silica (only through the 13 mm orifice), and for potato starch, and in Figure 13a for silica (only through the 30 mm orifice), and for corn starch. The final values of the discharged mass in Figure 10, and in the other mass-time series generally did not correspond to the loaded mass of solids due to a residual mass in the bin at the end of the discharge. Values of these residual masses relative to the loaded mass are given in Figure 11b to Figure 13b, as a function of the aeration rate for the same materials. All the powders in these picture show a

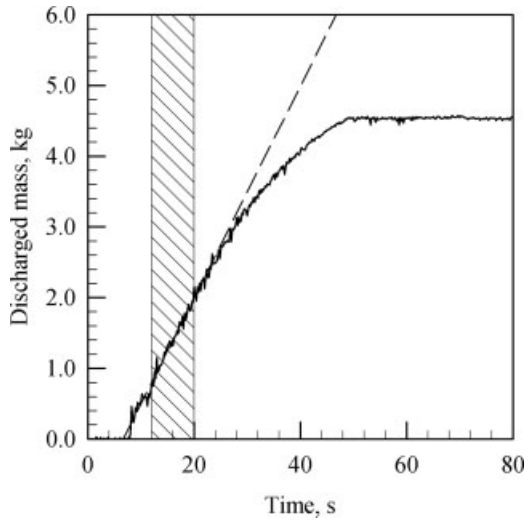

Figure 10. Mass of discharged solids as a function of time for the 15 μm magnesium carbonate powder at u = 21 mm s^{-1}:——, experimental data; — — — linear interpolation of data in the constant discharge rate range within the dashed area.

threshold value of aeration below which the powders do not discharge. This phenomenon can be associated to the formation of stable structures, such as domes or pipes within the solids that stop the flow. Aeration promotes gas pressure gradients favorable to the solids flow which can determine the powder motion. The understanding of this phenomenon and the prediction of the aeration rate at which this happens will be the object of further studies.

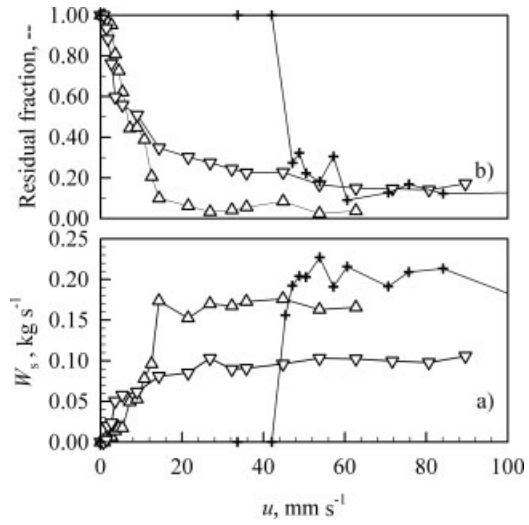

Figure 11. Solids discharge rate and residual mass as a function of the aeration rate: +calcium carbonate, 30 mm orifice; △, 15 μm magnesium carbonate, 13 mm orifice; ▽, 4 μm magnesium carbonate, 13 mm orifice.

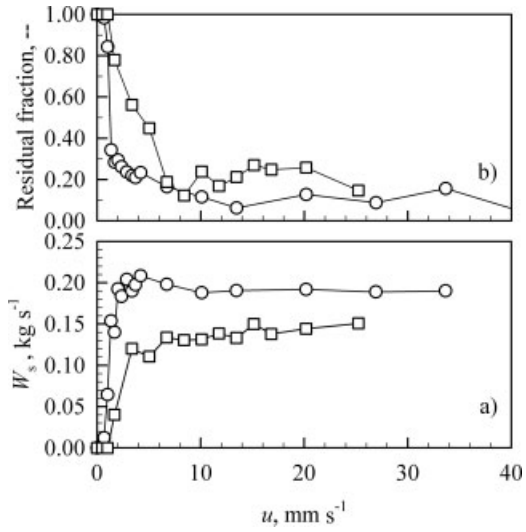

Figure 12. Solids discharge rate and residual mass as a function of aeration rate: ○, silica, 13 mm orifice; □, potato starch, 13 mm orifice.

Comparison between the plot of the discharge rate as a function of the aeration rate and the fluidization curves for the same powder shows that the attainment of the maximum value of the solid discharge rate corresponds to the effective solid fluidization. This is in agreement with what has been found to date on the effects of aeration.[13]

Visualization of the discharging stream

Single images of discharging solids were taken at different aeration rates. Some examples for most of the tested materials are shown in Figure 14. Aggregates are very fragile and most of them can breakup in the discharge process. However, the largest aggregates which are found in the discharging stream should be representative of the aggregates present in the silo. All these aggregates measured showed sizes of a few millimeters in accordance with what had been observed in Figure 9. The discharge of aggregates also appeared at aeration rates at which they could not be detected by inspection of the fluidization column. The size of the discharging aggregates did not appear to be significantly affected by the aeration rate.

Discussion

Some of the fluidization and discharge features described before for the tested powders differ considerably from what had been previously observed by Donsì et al.[13] and reported in the introduction. Indeed, the fluidization behavior of all the carbonates and of the silica powder shows an inversion in the sequence of fluidization and channeling velocity ranges. In particular, the shapes of those fluidization curves are similar to those reported by Wang et al.[15] for limestone. Also in that case the reported size of aggregates was larger than 1 mm. As noted before, all the powders tested in this work show a threshold value of aeration in order for discharge to start.

According to what is discussed in the Theoretical Background section, the procedure suggested by Donsì et al.[14] was followed. Data relative to the fluidization of the different powders were elaborated using Eqs. 8 and 11 to 14. In particular, a regression procedure was applied with the objective of finding the best choice for ε_i, which minimizes the sum of relative square deviations between diameters evaluated for each powder according to Eq. 8, and those evaluated for the same powder solving the system of Eqs. 11 to 14 at each aeration condition in the fluidization range. Aggregate diameters and densities resulting from this calculation are reported in Table 3. The evaluated aggregate diameters are all between 1 and 6 mm, and appear satisfactorily close to the observed size of aggregates. Densities of aggregates are always larger than bulk densities of the powders, and in a range between 1 and 1.4 times this value. External voidage values are given in Figure 15a to Figure 17a as a function of the aeration rate. As it is clear from these figures, most of these data are in the range between 0.2 and 0.4, and can be as low as 0.1 at low-aeration rates. These voidage values represent the bed-volume fraction occupied by voids between the aggregates, and, therefore, are not comparable with the usual voidage values of 0.35 and of larger beds of predominantly spherical particles. In this case, in fact, these voids derive from the gradual separation of aggregates and assume reticular low-voidage configurations, such as those shown in the pictures in Figure 9. In principle, the external voidage can approach zero when the aggregates are compacted by an external load. Comparison of experimental discharge rates and those predicted by using Eqs. 4 and Eq. 18 is given in Figure 15b to Figure 17b. In order to cover the wide variations of the solids discharge rates obtained by the different techniques a log scale is adopted. This representation does

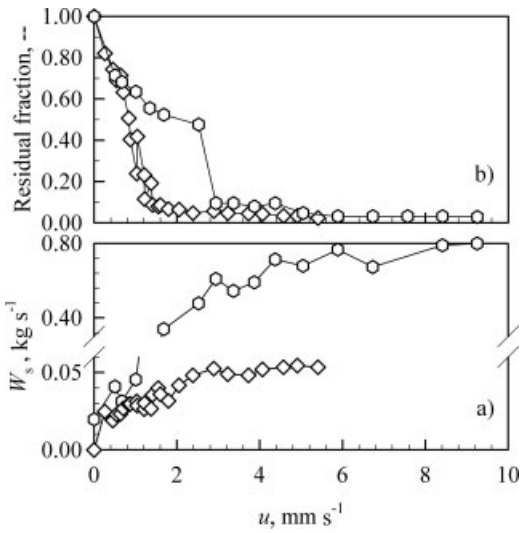

Figure 13. Solids discharge rate and reduced mass as a function of aeration rate: ⬡, silica, 30 mm orifice; ◇, corn starch, 13 mm orifice.

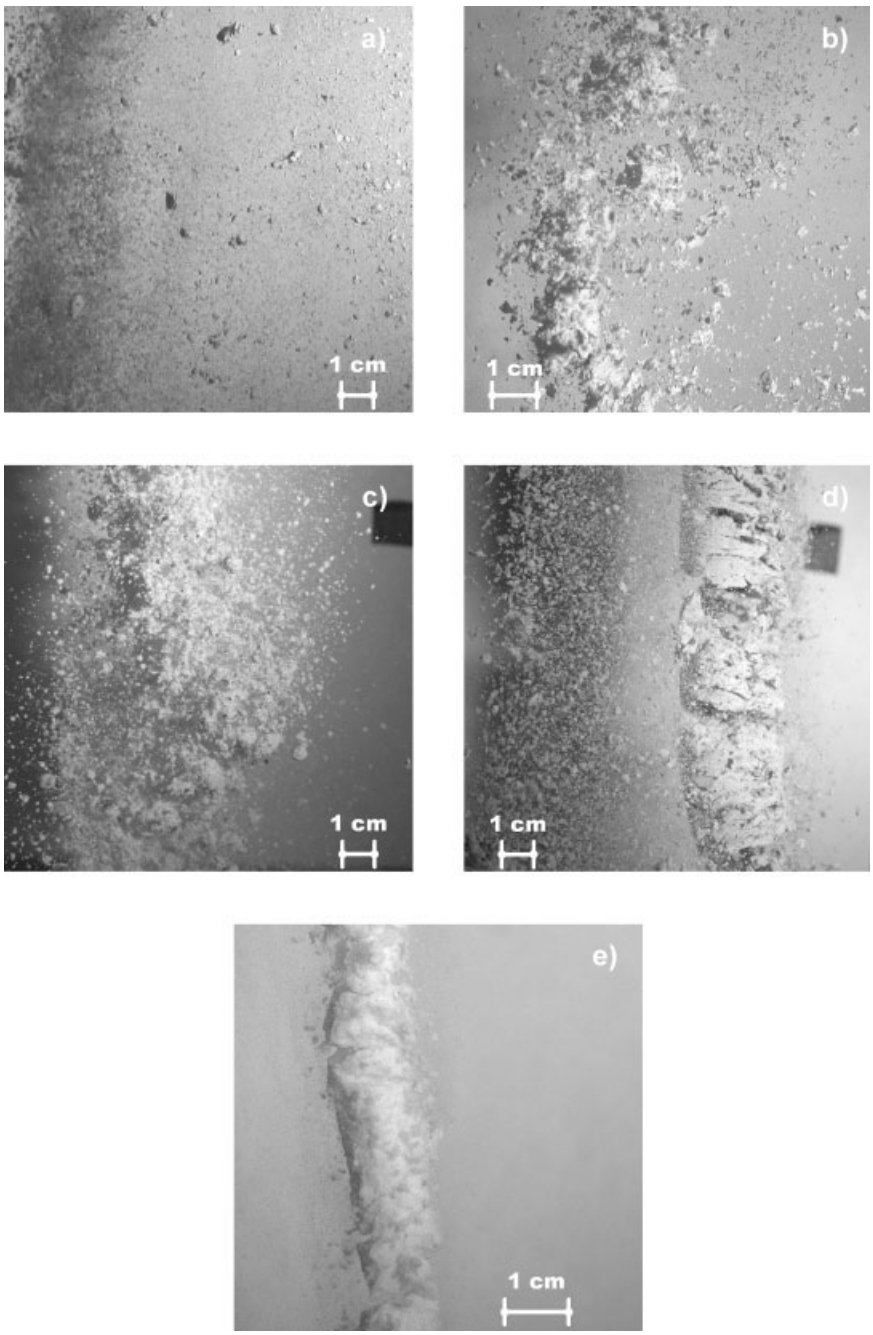

Figure 14. Aggregation during discharge: (a) calcium carbonate; (b) 15 μm magnesium carbonate; (c) 4 μm magnesium carbonate; (d) silica and (e) potato starch.

not allow to visualize zero flow points at aeration rates below the minimum for the discharge, for which this comparison is meaningless. Inspection of the figures reveals that Eq. 4, based on a single particle discharge model, largely overpredicts the experimental results. Instead, Eq. 18, accounting for powder aggregation, generally underpredicts the experimental results. However, the relative deviation of discharge rates between model evaluation and experimental results is smaller when using Eq. 18, than those obtained when using Eq. 4.

Aggregate density calculated starting from fluidization data, and reported in Table 3 compares fairly well with the measured vibrated density of the powders, as if powder vibration causes perfect compaction of the aggregates bringing the external voidage value to zero. Therefore, in the absence of fluidization experiments, the vibrated density can be a reasonable estimate of the aggregate density. This value can be used to evaluate the aggregate diameter and the voidage external to the aggregates according to Eqs. 15 to 17, and, in turn, to estimate the solids discharge rate with Eq. 18.

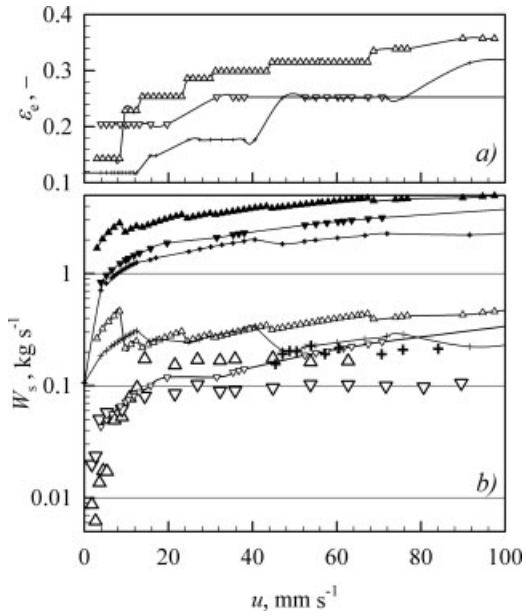

Figure 15. Voidage value external to the aggregates (a) and solids discharge rate, (b) as a function of aeration rate.

Voidage values in (a) were evaluated according to Eqs. 8 and 11 to 14, following the procedure given in the text: +—+—+, calcium carbonate; △—△—△, 15 μm magnesium carbonate; ▽—▽—▽, 4 μm magnesium carbonate. Solids discharge rates in (b). Experimental data: +, calcium carbonate, 30 mm orifice; △, 15 μm magnesium carbonate, 13 mm orifice; ▽, 4 μm magnesium carbonate, 13 mm orifice. Single particle-discharge model (Eq. 4): +—+—+, calcium carbonate; ▲—▲—▲, 15 μm magnesium carbonate, 13 mm orifice; ▼—▼—▼, 4 μm magnesium carbonate, 13 mm orifice. Aggregate discharge model equation (18): +—+—+, calcium carbonate, 30 mm orifice; △—△—△, 15 μm magnesium carbonate, 13 mm orifice; ▽—▽—▽, 4 μm magnesium carbonate, 13 mm orifice.

Figure 18 reports a parity check between the experimental data and results of the three models proposed. Namely these are: (a) the simplified aggregative discharge model according to which the evaluation of the discharge rate is given by Eq. 18, with the aggregate density set to the vibrated density value, and aggregate size and external voidage calculated from Eqs. 16 and 17, respectively; (b) the complete aggregative discharge model according to which the evaluation of the discharge rate is given by Eq. 18, with aggregate density, aggregate size and external voidage obtained from fluidization data elaborated according to the procedure, using Eqs. 8 and 12 to 14, (c) and the single particle discharge model equation (Eq. 2). This comparison indicated that the simplified aggregative discharge model a, is less precise than the more complete model b. However, despite its simplicity, the simplified aggregative discharge model a, provides us with satisfactory results for all the material tested, producing errors that are generally lower than 40%. Both aggregative discharge models a and b, show a generally much better agreement with experimental data than the single particle model c. This indicates that the procedure proposed by Donsì et al.[14] and summarized in the Theoretical Background section of this article, is able to predict the solid discharge rate of a cohesive solid subject to aeration if an estimate of the aggregate diameter and voidage external to the aggregates is provided. In this respect, fluidization experiment can provide useful information on the bed permeability that can be used to uncouple the combined effect of aggregate density and aggregate size on the force balance of Eq. 8, describing the aggregate formation. In alternative to fluidization experiments, vibrated density can be a good estimate of the aggregate density to be used to implement the force balance as in Eq. 16 to predict the aggregate diameter.

Conclusions

- Aeration successfully improved the discharge of a number of cohesive powders characterized by different flow properties, as revealed by shear test measurements and different fluidization behaviors. For the powders tested, aeration is able to overcome cohesive doming and piping. Further research is required for a better understanding and prediction of the critical aeration rate needed to reach this condition.
- Similarly to what was found by Wang et al.[15] our direct observation of the fluidized solids highlighted the presence

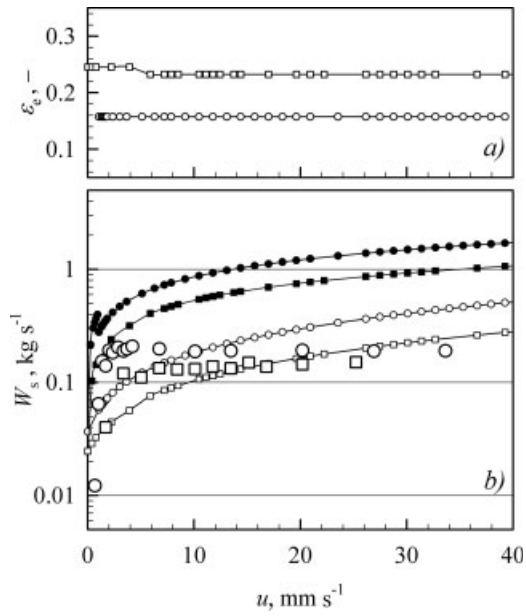

Figure 16. Voidage value external to the aggregates (a) and solids discharge rate (b) as a function of aeration rate.

Voidage values in (a) were evaluated according to Eqs. 8 and 11 to 14, following the procedure given in the text: ○—○—○, silica, 13 mm orifice; □—□—□, potato starch, 13 mm orifice. Solids discharge rates in (b). Experimental data: ○, silica, 13 mm orifice; □, potato starch, 13 mm orifice. Single particle discharge model equation (Eq. 4): ●—●—●, silica, 13 mm orifice; ■— ■— ■, potato starch, 13 mm orifice. Aggregate discharge model equation (Eq. 18): ○—○—○, silica, 13 mm orifice; □—□—□, potato starch, 13 mm orifice.

of clearly formed aggregates of a few millimeters in size. The presence of these aggregates was also detected in the discharging stream by means of digital photography coupled with stroboscopic lighting.

- Coupling data relative to the powder tensile strength and the pressure drop and mass balances through the fluidized bed, it was possible to correctly estimate the aggregate size simply by making straightforward hypotheses on the aggregate formation and their effects on aeration.
- Vibrated density turned out to be a good estimate of the aggregate density. This implies that for these powders the main effect of vibration is to change the spatial organization of aggregates within the powder.
- The de Jong and Hoelen[9] equation modified by Donsì et al.[14] provides good estimates of the solids discharge rates. The role of aggregates in the aerated powder discharge is confirmed by this study. Simply by accounting for their presence, in fact, solids discharge rates can be reasonably predicted.
- The measurement of vibrated density and the powder shear measurements with a standard Schulze cell extrapolated to zero consolidation, can provide the necessary data for a fairly simple procedure to predict the solids discharge rate under aerated conditions.

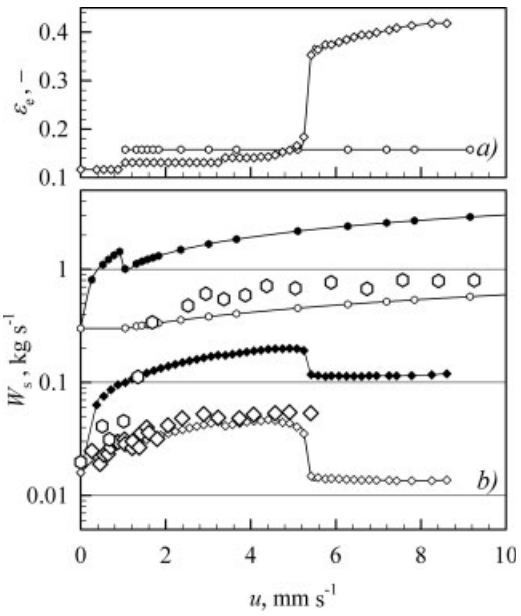

Figure 17. Voidage value external to the aggregates (a) and solids discharge rate (b) as a function of aeration rate.

Voidage values in (a) were evaluated according to Eqs. 8 and 11 to 14 following the procedure given in the text: ⬡—⬡—⬡, silica, 30 mm orifice; ◇—◇—◇, corn starch, 13 mm orifice. Solids discharge rates in (b). Experimental data: ⬡, silica, 30 mm orifice; ◇, corn starch, 13 mm orifice. Single particle discharge model equation (Eq. 4): ⬢—⬢—⬢, silica, 30 mm orifice; ◆—◆—◆, corn starch, 13 mm orifice. Aggregate discharge model equation (Eq. 18): ⬡—⬡—⬡, silica, 30 mm orifice; ◇—◇—◇, corn starch, 13 mm orifice.

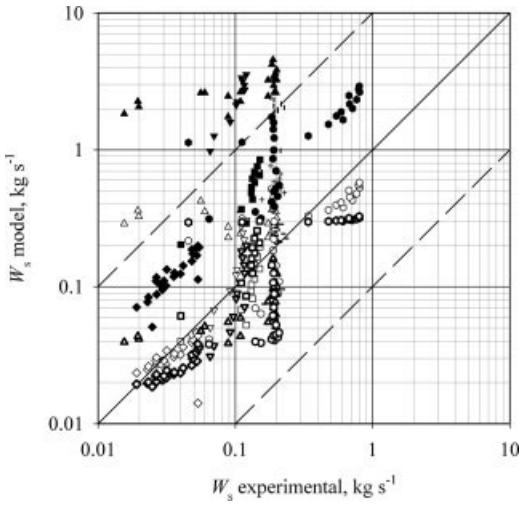

Figure 18. Parity plot for: (a) the simplified aggregative discharge model according to which the evaluation of the discharge rate is given by Eq. 18, with the aggregate density set to the vibrated density value, and aggregate size and external voidage calculated from Eqs. 16 and 17, respectively (hollow symbols with thick walls); (b) the complete aggregative discharge model according to which the evaluation of the discharge rate is given by Eq. 18 with aggregate density, aggregate size and external voidage obtained from fluidization data elaborated according to the procedure using Eqs. 8 and 12 to 14 (hollow symbols); (c) the single particle discharge model equation (Eq. 2) (filled symbols).

Acknowledgments

This research work was partially financed by the Italian Ministry of research within the framework of a Prin (Year 2003) Project. This work was also partially sustained by a free research Grant provided by DuPont. In particular the scientific inspiration of Dr. Tim Bell of the same Company is gratefully acknowledged. The authors also wish to thank Mr. Luigi Esposito for helping with particle-size distribution, and Ms. Lucia Liguori for helping with some of the experiments. The authors are grateful to MiMac (Italy) for providing with the magnesium carbonate powders.

Notation

a = permeability parameter in Eq. 2
a' = permeability parameter in Eq. 8
a_s = specific surface area, m^2 kg^{-1}
b = permeability parameter in Eq. 2
b' = permeability parameter in Eq. 8
c = cohesion, Pa
c_0 = cohesion, extrapolated to zero consolidation, Pa
D_c = fluidization column diameter, m
D_s = silo diameter, m
F_c = contact force, N
d_a = aggregate mean diameter, m
d_o = bin outlet diameter, m
d_p = particle Sauter mean diameter, m
d_{p10} = 10th percentile diameter in particle-size distribution, m
d_{p50} = 50th percentile diameter in particle-size distribution, m
d_{p90} = 90th percentile diameter in particle-size distribution, m

d_{pv} = particle volume mean diameter, m
g = acceleration due to gravity, m s^{-2}
H = solids height, m
k = number of the effective contacts between an aggregate and its neighbors on another layer
m_b = loaded mass of solids in the bed, kg
m_s = loaded mass of solids in the silo, kg
n_c = contact density, m^{-2}
Q_f = aeration rate, m^3 s^{-1}
Q_{fo} = gas-volumetric flow rate through the orifice, m^3 s^{-1}
Q_{so} = solid-volumetric flow rate, m^3 s^{-1}
u = gas-superficial velocity, m s^{-1}
u_e = gas velocity in the voidage external to the aggregates, m s^{-1}
u_i = gas velocity within the aggregates, m s^{-1}
W_s = solids discharge rate, kg s^{-1}

Greek letters

Δp = pressure drops through the bed, Pa
ε_b = voidage of the bulk solids
ε_e = voidage between aggregates
ε_i = voidage within aggregates
μ_f = gas viscosity, Pa s
ρ_a = aggregate density, kg m^{-3}
ρ_b = powder bulk density, kg m^{-3}
ρ_{b0} = powder bulk density extrapolated at zero consolidation, kg m^{-3}
ρ_{bv} = vibrated powder bulk density, kg m^{-3}
ρ_f = gas density, kg m^{-3}
ρ_p = particle density, kg m^{-3}
Σ = bed cross-section, m^2
σ = normal stress, Pa
σ_1 = major principal stress, Pa
σ_t = tensile strength, Pa
τ = shear stress, Pa
ϕ = angle of internal friction, deg
ϕ_0 = angle of internal friction extrapolated to zero consolidation, deg

Literature Cited

1. Crewdson BJ, Ormond AL, Nedderman RM. Air-impeded discharge of fine particles from a hopper. *Powder Technol*. 1977;16:197–207.
2. Beverloo WA, Leniger HA, van de Velde J. The flow of granular material through orifices. *Chem Eng Sci*. 1961;15:260–269.
3. Geldart D. Types of gas fluidization. *Powder Technol*. 1973;7:285–292.
4. Geldart D, Williams JC. Flooding from hoppers: Identifying powders likely to give problems. *Powder Technol*. 1985;43:181–183.
5. Jenike AW. *Gravity flow of bulk solids*. Bulletin n.108 of the Utah Engineering Experimental Station, University of Utah, Salt Lake City, UT. 1961:52;29.
6. Ouwerkerk CED, Molenaar HJ, Frank MJW. Aerated bunker discharge of fine dilating powders. *Powder Technol*. 1992;72:241–253.
7. Ferrari G, Bell TA. Effect of aeration on the discharge behavior of powders. *Powder Handling and Processing*. 1998;10:269–274.
8. Altiner HK. Flow of solids from aerated hoppers: effect of aeration methods. *AIChE Symp Ser*. 1983;222:55–59.
9. De Jong JAH, Hoelen QEJJM. Cocurrent gas and particle flow during pneumatic discharge from a bunker trough an orifice. *Powder Technol*. 1975;12:201–208.
10. Massimilla L, Betta V, Della Rocca CA. Study of streams of solids flowing from solid-gas fluidized beds. *AIChE J*. 1961;7:502–508.
11. Kurtz HP, Rumpf H. Flow processes in aerated silos. *Powder Technol*. 1975;11:147–156.
12. Jochem K, Schwedes J. Aeration discharge aid for silos. *Proceedings of the 3rd World Congress on Particle Technology*. Brighton, UK. July 6–9, 1998:322.
13. Donsì G, Ferrari G, Poletto M, Russo P. Gas pressure measurements inside an aerated hopper. *Chem Eng Res Des*. 2004;82:72–84.
14. Donsì G, Ferrari G, Poletto M, Russo P. Aggregative behavior of cohesive magnesium carbonate powders in fluidization and aerated discharge. *KONA*. 2003;21:54–66.
15. Wang Z, Kwauk M, Li H. Fluidization of fine particles. *Chem Eng Sci*. 1998;53:377–395.
16. Pacek AW, Nienow AW. Fluidisation of very dense hardmetal powders. *Powder Technol*. 1990;60:145–158.
17. Mikami T, Kamiya H, Horio M. Numerical simulation of cohesive powder behavior in a fluidized bed. *Chem Eng Sci*. 1998;53:1927–1940.
18. Russo P, Chirone R, Massimilla L, Russo S. The influence of the frequency of acoustic waves on sound-assisted fluidization of beds of fine particles. *Powder Technol*. 1995;82:219–30.
19. Rumpf H. The strength of granules and agglomerates. In: Knepper WA. *Agglomeration*. New York: John Wiley & Sons, Inc; 1962: 379–418.
20. Kendall K, Alford NMcN, Birchall JD. Elasticity of particle assemblies as a measure of the surface energy of solids. *Proc R Soc Lond*. 1987;A412:269–283.
21. Schulze D. Measurement of the flowability of bulk solids. In: Brown CJ, Nielsen J. *Silos*. London: E&F Spon; 1998:18–52.
22. Krupp H. Particle adhesion theory and experiment. *Advan Colloid Interface Sci*. 1967;1:111–239.
23. Suzuki M, Sato H, Hasegawa M, Hirota H. Effect of size distribution on tabbing properties of fine powders. *Powder Technol*. 2001;118:53–57.

Manuscript received Dec. 1, 2006, and revision received Apr. 3, 2007.